First-principles analysis on interface mismatch relationship between La_2O_3 and TiC

Weidong Ma [a,b], Tianfang Zhu [a], Hanqi Wang [c], Yefei Zhou [b,*], Ligang Liu [b,**], Xuejun Ren [d], Qingxiang Yang [a,***]

[a] *State Key Laboratory of Metastable Materials Science & Technology, Hebei Key Lab for Optimizing Metal Product Technology and Performance, Yanshan University, Qinhuangdao, 066004, PR China*
[b] *College of Mechanical Engineering, Yanshan University, Qinhuangdao, 066004, PR China*
[c] *College of Mechanical Engineering, Qilu University of Technology, Jinan, 250353, PR China*
[d] *School of Engineering, Liverpool John Moores University, Liverpool, L3 3AF, UK*

Abstract

Hypereutectic Fe-Cr-C alloy was widely applied in the field of additive manufacturing. By adding TiC, the wear resistance of the alloy can be further enhanced. Based on the hypereutectic Fe-Cr-C-Ti alloy, rare earth oxide La_2O_3 will be added to refine TiC. The first-principles method was used to calculate the interface adhesion work, interface energy, electronic structure and bonding properties between La_2O_3 and TiC. The effectiveness of La_2O_3 as the nucleation substrate of TiC was also analysed in this paper. The calculation results show that the mismatch degree between the TiC(1 $\bar{1}$ 0) plane and the La_2O_3(1 $\bar{1}$ 0) plane is 4.10%, which meets the necessary condition for heterogeneous nucleation. It indicates that the TiC(1 $\bar{1}$0) plane can rely on the La_2O_3(1 $\bar{1}$ 0) plane for heterogeneous nucleation. The TiC(1 $\bar{1}$ 0) surface is a non-polar surface and has only one stacking mode. The TiC(1 $\bar{1}$ 0) surface converges after 8 layers, with the surface energy is 3.510 J/m^2. The O-terminated type of La_2O_3(1 $\bar{1}$ 0) converges at the 28th layer on the surface, with the surface energy of 1.481 J/m^2. The O-La- terminated surface of La_2O_3(1 $\bar{1}$ 0) converges at the 10th layer, with a surface energy value of 2.276 J/m^2. In the La_2O_3(110)/TiC(110) interface model, the interface adhesion work of O-La terminated interface model is the largest, which is 0.51 J/m^2, while the interface energy of O-La terminated interface model is the smallest, which is 5.28 J m^{-2}. Therefore, La_2O_3 meets the conditions to serve as the nucleation substrate of TiC and is inclined to form an O-La terminated hetero-nucleation interface, thereby refining TiC.

1. Introduction

In recent years, the additive manufacturing has been widely applied in many fields such as aerospace, automotive, and shipbuilding [1,2], in which, Fe-alloy has gained attention in the additive manufacturing industry due to its comprehensive mechanical properties and relatively low cost [3,4]. The hypereutectic Fe-Cr-C alloy exhibits excellent wear resistance and has been widely applied in the additive manufacturing field [5–7]. In the hypereutectic Fe-Cr-C-Ti alloy, M_7C_3(M = Fe,Cr) and TiC carbides are main strengthening phases, which are dispersed and distributed on the surface of the alloy, and the wear resistance of the alloy is further enhanced [8,9]. However, during the service period, as the external load increases, some larger-sized M_7C_3 and TiC carbides particles will flake off from the surface of the alloy, thereby reducing

its service life [10,11]. Therefore, how to refine M_7C_3 and TiC carbides particles in the hypereutectic Fe-Cr-C-Ti alloy is the key to improving the service performance of the alloy.

Among the rare earth oxides, La_2O_3 has attracted attention due to its excellent properties and abundant reserves in nature. It was added as an additive to alloys to improve the mechanical properties of the alloys [12, 13]. Y. H. Chen et al. [14] investigated the addition of La_2O_3 on grain refinement of additive manufactured Ti-6.5Al-3.5Mo-1.5Zr-0.3Si titanium alloy. The results show that the La_2O_3 addition can significantly refine the size of the prior β grains. J. Yang et al. [15] studied the microstructure and wear resistance of the hypereutectic Fe-Cr-C alloy with different La_2O_3 additives. In our previous work, the refinement mechanism of the primary M_7C_3 carbide by La_2O_3 was Cr–C alloy decreases gradually. However, La_2O_3 was added to the hypereutectic Fe-Cr-C-Ti alloy, the refinement of TiC has not been reported. Moreover, it is very difficult to apply experimental methods to determine the interface relationship between La_2O_3 and TiC in the hypereutectic Fe-Cr-C-Ti alloy, thereby revealing the mechanism by which La_2O_3 refines the TiC.

Currently, the first-principles method has been widely applied in the study of material surface and interfaces, and it explains the bonding characteristics between atoms from the perspective of electronic structure [17,18]. B. F. Chen et al. [19] systematically investigated alloying effects on interfacial bonding characteristics in $Fe_3C(001)/\alpha'C(112)$ heterostructures using first-principles calculations. W. Y. Huang et al. [20] calculated the behaviours of H atoms and vacancies at the W/Lu_2O_3 interface using first-principles calculations. Recently, some references about the first-principles study of carbide/oxide interfaces and the fundamental theory of DFT have been reported. H.Y. Hwang et al. [21] investigated the SiC/SiO_2 interface, and it was explained that the introduction of oxygen can significantly affect electron scattering even in the absence of electrically active defects. L. Wang et al. [22] considered the influence of the intercalation of SiC and TiC on the epitaxial growth of graphene on SiC, and the interfacial bonding and thermodynamic stability were revealed. Therefore, in this paper, the first-principles method was employed to explain the interface structure and interface bonding strength between La_2O_3 and TiC at the atomic scale, and it is demonstrated that the mechanism by which La_2O_3 refines TiC is feasible, which can provide a theoretical basis for the preparation of the hypereutectic Fe–Cr–C-Ti alloys containing fine-sized TiC carbides.

This first-principles method was employed in this paper. The interface adhesion work, interfacial energy, electronic structure and bonding properties between La_2O_3 and TiC carbides were calculated, and the effectiveness of La_2O_3 as the nucleation substrate of TiC was analysed.

2. Computational details

The Vienna Ab Initio Simulation Package (VASP) based on density functional theory [23] was adopted to optimize the bulk structures of La_2O_3 and TiC, and to calculate their surface and interface properties in this paper. The exchange-correlation energy was calculated and corrected using the generalized gradient approximation (GGA) functional improved by Perdew, Burke and Ernzerhof (PBE) [24].

The interaction between the ionic nuclei and valence electrons was described by the projector augmented wave (PAW) method [25]. The appropriate plane wave energy cutoff (E_{ncut}) and Brillouin zone K-point grid were selected by convergence tests.

The effect of E_{ncut} and K-points on the bulk phase of TiC is shown in Fig. 1. Fig. 1(a) shows the E_{ncut} variation of TiC as a function of the energy. When the E_{ncut} reaches 500 eV, the energy converges and the bulk phase energy stabilizes at −77.78 eV.

Fig. 1 (b) shows the K-point of TiC as a function of energy. It can be observed that after setting the K-point to 9 × 9 × 9, the energy converges and the bulk phase energy stabilizes at approximately −77.81 eV. Therefore, the E_{ncut} and K-point of TiC should be set to 500 eV and 9 × 9 × 9 respectively.

The effect of E_{ncut} and K-points on the bulk phase of La_2O_3 is shown in Fig. 2. Fig. 2(a) shows the E_{ncut} variation of La_2O_3 as a function of the energy. When the E_{ncut} reaches 500 eV, the energy converges and the bulk phase energy stabilizes at −41.81 eV. Fig. 2 (b)shows the K-point of La_2O_3 as a function of energy. It can be observed that after setting the K- point to 7 × 7 × 7, the energy converges and the bulk phase energy stabilizes at approximately −41.88 eV. Therefore, the E_{ncut} and K-point of La_2O_3 should be set to 500 eV and 7 × 7 × 7 respectively.

3. Results and analysis

3.1. Effect of C vacancy on the thermodynamic stability of TiC

The thermodynamic stability of TiC has a significant impact on the interface properties of La_2O_3 and TiC. The formation energy of TiC ($TiC_{1.00}$) with 10%, 25% and 33% C vacancies, which can be named as $TiC_{0.90}$, $TiC_{0.750}$ and $TiC_{0.67}$, were calculated in this paper.

The calculations presented here have been made using a full- potential linear muffin-tin orbital method (FP-LMTO) within the local density approximation (LDA) of density functional theory [26,27]. In order to study the cubic phase for several stoichiometries, from $TiC_{1.00}$ to $TiC_{0.67}$, a supercell with an fcc lattice and a basis with 8 titanium atoms and 8 carbon atoms. The carbon atoms were subsequently removed creating $TiC_{1.00}$, $TiC_{0.90}$, $TiC_{0.75}$ and $TiC_{0.67}$ were created.

The formation energy can be defined as follow:

$$E_{form} = \frac{E(Ti_mC_n) - mE(Ti_{hcp}) - nE(C_{grapite})}{n+m} \quad (1)$$

where n and m are the number of nonmetal and metal atoms used in the super cell, was calculated for the structures and stoichiometries studied.

The formation energies as a function of carbon vacancies for all TiC phases with different C vacancies are listed in Table 1. From Tables 1 and it can be seen that the formation energies of $TiC_{1.00}$ is the smallest, which indicates that TiC is the most stable. The calculation results are in agreement with Reference [28]. Therefore, TiC can be used to calculate the interface properties of La_2O_3 and TiC.

3.2. Crystal structure and bulk properties of La2O3 and TiC

The crystal structures of La2O3 and TiC are shown in Fig. 3. Fig. 3(a) is the crystal structure of La2O3, with lattice constants a = b =3.926 Å and c =6.123 Å. Fig. 3(b) is the crystal structure of TiC, with lattice constant a = 4.33Å.

The calculated phase properties of La_2O_3 are shown in Fig. 4. Fig. 4 (a) is the energy band structure of La_2O_3. The position indicated by the red dotted line represents the Fermi level. From Fig. 2(a), the energy band of La_2O_3 does not pass through the Fermi level, and there is a certain band gap width between the valence band and the conduction band. The band gap energy is 3.86 eV, which indicate that it exhibits certain semiconductor properties. Fig. 4(b) is the density of states diagram of La_2O_3. It is clearly observable that the s orbitals of O and the p orbitals of La have resonance, which indicates that it has certain covalent bond properties. Moreover, the centre of gravity of La's d orbitals is not consistent with that of O's p orbitals, which suggests the presence of strong ionic bonds. Therefore, the chemical bond interaction in the La_2O_3 crystal structure is a combination of covalent bonds and ionic bonds.

The calculated phase properties of the TiC are shown in Fig. 5. Fig. 5 (a) is the energy band structure of TiC. Fig. 5(b) is the density of states obtained based on the energy band structure. The position indicated by the dotted line represents the Fermi level. As shown in Fig. 5(a), the energy band passes through the Fermi level, which indicates that TiC exhibits metallic properties. In Fig. 5(b), the d orbitals of Ti overlap with the p orbitals of C. Particularly, there is a significant resonance in the energy range from − 6 eV to the Fermi level, which indicates that there are p-d hybridization orbitals between C and Ti, thereby forming covalent bonds. However, the centre of the gravity of states of the d orbitals of Ti and the p orbitals of C are not consistent, which suggests that there are still certain ionic bonds between TiC and C. Therefore, the bonding of TiC is a combination of metallic bonds, covalent bonds and ionic bonds.

3.3. Surface property of La_2O_3 and TiC

3.3.1. Mismatch degree calculation

According to Bramfitt 2D lattice mismatch theory [29], if the 2D lattice mismatch between the basal phase and the nucleating phase is less than 6%, the basal phase is able to play a very effective heterogeneous nucleation role with respect to the nucleating phase; with the mismatch degree of 6-12%, the basal phase plays a moderately effective heterogeneous nucleation role with respect to the nucleating phase; and the mismatch degree is larger than 12%, the basal phase cannot act as a heterogeneous nucleus for the nucleating phase. The two-dimensional lattice mismatch is calculated as follows [29]:

$$\delta_{(hkl)_n}^{(hkl)_s} = \sum_{i=1}^{3} \left[\left(\left| d_{[uvw]_s}^{i} \cos\theta - d_{[uvw]_n}^{i} \right| \Big/ d_{[uvw]_n}^{i} \right) \Big/ 3 \right] \times 100\% \qquad (2)$$

where, $(hkl)_s$ is a low-index crystal plane in the nucleation substrate; $[uvw]_s$ is a low-index crystal direction in the low-index crystal plane of the nucleation substrate; $(hkl)_n$ is a low-index crystal plane in the nucleation phase; $[uvw]_n$ is a low-index crystal direction in the low- index crystal plane of the nucleation phase; $d_{[uvw]n}$ is the distance of atoms in the crystal plane of $(hkl)_n$ along the direction of $[uvw]_n$; $d_{[uvw]s}$ is the atomic distance along the $[uvw]_s$ direction in the $(hkl)_s$ crystal plane. θ is the angle between $[uvw]_n$ low-index crystal direction and $[uvw]_s$ low-index crystal one.

The low-index crystal planes of La_2O_3/TiC, namely La_2O_3 (110)/TiC (110), La_2O_3 (001)/TiC (100) and La_2O_3 (110)/TiC (110) were selected, and their misfit relationships were calculated. The results are listed in Table 2. The mismatch degree of the crystal plane of La_2O_3 (110)/TiC (110) is the smallest, which is 4.10%. It is a coherent interface. This proves that La_2O_3 and TiC can form a hetero-interface, and La_2O_3 can serve as the core for the heterogeneous nucleation of TiC.

3.3.2. TiC surface convergence test

TiC(1 1 0) surface is a non-polar surface, and its surface energy formula is as follows [30]:

$$\sigma = \frac{1}{2A}\left(E_{slab}^{N} - N\Delta E\right) \qquad (3)$$

$$\Delta E = \left(E_{slab}^{N} - E_{slab}^{N-2}\right) / 2 \qquad (4)$$

where N represents the number of atomic layers on the surface model; E_{slab}^{N} represents the total energy of the surface model system with N layers of atoms; E_{slab}^{N-2} represents the total energy of the surface model system with N-2 layers of atoms; A is the stacking area of the surface model.

Since the TiC (1 1 0) surface is a non-polar surface, its stacking mode is unique, as shown in Fig. 6. The surface energy was calculated, and the results are listed in Table 3. The TiC (1 1 0) surface converges at 8 layers, and the surface energy is 3.510 J/m^2.

3.3.3. La_2O_3 surface convergence test

The chemical potential calculation formula for the La_2O_3 surface model is as follows [30]:

$$\mu_{La_2O_3}^{bulk} = 2\mu_Y + 3\mu_O \quad (5)$$

Where μ_{La2O3}^{bulk} represents the energy of the system after the structural relaxation of La_2O_3 (1 1 0); μ_{La} represents the chemical potential of the La atom; μ_O represents the chemical potential of the O atom.

The surface energy formula for calculating the La_2O_3 (1 1 0) surface is as follows [30]:

$$\sigma = \frac{1}{2A}(E_{slab} - N_{La}\mu_{la} - N_O\mu_O) \quad (6)$$

where E_{slab} represents the energy value (J) of the surface model with a certain number of atomic layers; A represents the surface area of the model (m^2); N_{La} and N_O represent the number of La and O atoms in La_2O_3 (1 1 0) surface model respectively.

By combining Equations (4) and (5), the final surface energy calculation formula for the surface model on the La_2O_3 (1 1 0) plane is as follows:

$$\sigma = \frac{1}{2A}\left[E_{slab} - \frac{1}{2}N_{La}\mu_{La_2O_3}^{bulk} - \left(\frac{1}{2}N_{La}\text{-}4\right)\mu_O\right] \quad (7)$$

La_2O_3(1 1 0) surface is a polar one. When constructing the La_2O_3(1 1 0) surface model, the starting layering position is different, and the atoms at the termination surface are also different. By considering different atomic configurations at the termination surfaces, two types of slicing methods for the La_2O_3(1 1 0) surface are obtained, namely the O- atom terminated surface and the O-La atom terminated surface, as shown in Fig. 7. Fig. 7(a) is the schematic diagram of the O-La atom- terminated surface of La_2O_3(1 1 0). After calculating the surface energy, the data are presented in Table 4.

The surface energy of the La_2O_3(1 1 0) model with O-La atom terminated converges to 2.276 J/m^2 after 10 layers. Fig. 7(b) is the schematic diagram of the O atom terminated model on La_2O_3(1 1 0) surface. The surface energy was calculated, and the results are listed in Table 5. It can be known that the surface energy of the O atom terminated model of La_2O_3(1 1 0) converges at 28 layers, and the surface energy is 1.481 J/m^2.

3.4. Interfacial property

3.4.1. Interface connection method

Since the TiC(1 1 0) surface does not need to consider the positional correlation, when the La_2O_3(1 1 0) surface and the TiC (1 1 0) surface interface connect in the two termination cases, it is always the same situation, as shown in Fig. 8. Fig. 8(a) is the O-La terminated model, and Fig. 8(b) is the O terminated model. The dotted line indicates the interface.

3.4.2. Analysis of interface charge density and differential charge density

The charge density and differential charge density are used to calculate and analyse the charge density situation at the interface and the bonding mechanism between atoms, in which, the calculation formula for the differential charge density is as follows [30]:

$$\rho_d = \rho_{tot} - \rho_{La_2O_3} - \rho_{TiC} \quad (8)$$

where ρ_{tot} represents the total charge density (e/Å^3) in the interface model; ρ_{La2O3} and ρ_{TiC} represent the charge density (e/Å^3) of the individual La_2O_3 (110) layer and the TiC (110) layer within the same interface model.

The charge density distribution of the La_2O_3 (110)/TiC (110) inter-face is shown in Fig. 9. The dotted line represents the interface position. Fig. 9(a) is the charge density distribution of the O-La terminated interface along the (010) plane. It can be observed that the charge of the C atom above the interface significantly shifts downward towards the interface, which indicate that a chemical bond has formed between C and O at the interface. The charge of the La atom below the interface has a certain upward shift relative to the C atom above, which suggests that there is also a certain bond strength between them. Fig. 9(b) is the charge density of the model for the O-terminated interface. The cross- section is the (010) plane, and the interface position is marked by the dotted line. It can be clearly observed that there is a significant bonding behaviour between the C and O atoms near the interface.

The differential charge density diagram of the La_2O_3 (110)/TiC (110) interface is shown in Fig. 10. Fig. 10(a) is the differential charge density map of the O-La terminated interface obtained along the (010) plane.

It can be seen that on the left side near the interface, there is a concentration of charge on the side closer to the O atom between the O and C atoms, while there is a lack on the other side of the O atom. The C atom has a lack on the side closer to the O atom, while there is a concentration on the other side, which indicates that a polar covalent bond has formed between C and O. On the right side, there is a significant concentration of electrons between the La atom and the C atom, while there is an electron deficiency on the other side, which indicates that the bonding form between C and La is a combination of ionic bond and covalent bond.

Fig. 10 (b) is the differential charge density image of the O-terminated interface on the (010) plane. It can be observed that at the interface, the charges of the La atoms and C atoms on the right side are concentrated near the central part of the interface, while the La atoms on the other

side away from the interface show a phenomenon of charge deficiency. Therefore, there is a combination of strong polar covalent bonds and ionic bonds between La and C. On the left side, the O atoms also form ionic bonds and polar covalent bonds with the La atoms, and the O atoms are subject to dual bonding effects from La and the C atoms above the interface, which results in very obvious phenomena of charge deficiency and convergence on both sides.

In conclusion, by analysing the charge density and differential charge density at the interface, it can be concluded that regardless of the type of interface termination, effective bonding can occur at the interface, and the interface has good compatibility.

3.4.3. Interface adhesion work and interface energy

The interface adhesion work (W_{ad}) is an important parameter for characterizing the strength of interface bonding, in which, the formula for calculating the interface adhesion work of La_2O_3 (110)/TiC (110) interface model is as follows [31]:

$$w_{ad} = \frac{1}{A}\left(E_{TiC} + E_{La2_{O3}} - E_{TiC/La2_{O3}}\right) \quad (9)$$

where A is the interfacial area; E_{La2O3} is the total energy of La_2O_3 (110); E_{TiC} is the total energy of TiC (110); $E_{La2O3/TiC}$ is the total energy of La_2O_3 (110)/TiC (110) interface. The W_{ad} of La_2O_3 (110)/TiC (110) interface model is listed as Table 6. It can be seen that the W_{ad} of O-La termination interface model is the highest, which is 0.51 J/m^2. It indicates that this interface type has the strongest interface binding capability.

The interface energy (γ) represents the resistance encountered during the formation of a heterogeneous interface. The magnitude of the γ corresponds to the ease or difficulty of heterogeneous interface formation. The calculation formulas for γ in the two termination situation interface models are as follows [32]:

$$\gamma = \sigma_{TiC} + \sigma_{La2_{O3}} - w_{ad} \quad (10)$$

where σ_{La2O3} is the surface energy of La_2O_3 (110); σ_{TiC} is the surface energy of TiC (110).

The calculation results of the γ of La_2O_3 (110)/TiC (110) interface model are listed in Table 7. It can be seen that among the two interface models, the γ of the O-La terminated interface model constructed by the TiC (1 1 0) and La_2O_3(1 1 0) surfaces is the lowest, which is 5.28 J m^{-2}. Based on the calculation results of W_{ad} and γ, it is indicated that the W_{ad} of O-La terminated interface model is the highest and whose γ is the lowest. It is suggested that it possesses the best interface binding ability and relatively lowest interface nucleation resistance.

4. Conclusion

[1] La_2O_3 is a combination of covalent and ionic bonds, while TiC is a combination of metallic, covalent and ionic bonds.

[2] The mismatch degree between the TiC(1 1 0) plane and the La_2O_3(1 1 0) plane is 4.10%, which meets the necessary conditions for heterogeneous nucleation. It indicates that the TiC(1 1 0) surface can undergo heterogeneous nucleation relying on the La_2O_3(1 1 0) surface.

[3] The TiC(1 1 0) surface is a non-polar surface and has only one stacking mode. The TiC(1 1 0) surface converges after 8 layers, and the surface energy is 3.510 J/m^2. The O-terminated model of La_2O_3(1 1 0) converges at the 28th layer on the surface, and the surface energy is 1.481 J/m^2. The O-La-terminated model of La_2O_3(1 1 0) converges at the 10th layer, and the surface energy is 2.276 J/m^2.

[4] In the interface model of La_2O_3 (110)/TiC (110), the interface adhesion work of the O-La terminated model is the highest, which is 0.51 J/m^2, while the interface energy of the O-La terminated model is the lowest, which is 5.28 J m^{-2}. It indicates that it possesses the best interface binding ability and relatively lower interface nucleation resistance.

Credit authorship contribution statement

Weidong Ma: Conceptualization, Investigation, Methodology, Writing – original draft. **Tianfang Zhu:** Data curation, Visualization. **Hanqi Wang:** Methodology. **Yefei Zhou:** Methodology, Resources, Software. **Ligang Liu:** Methodology, Resources. **Xuejun Ren:** Funding acquisition, Project administration, Resources. **Qingxiang Yang:** Conceptualization, Investigation, Methodology, Resources, Software, Writing – review & editing.

Declaration of competing interest

The authors declare that they have no known competing financial interests or personal relationships that could have appeared to influence the work reported in this paper.

Acknowledgements

The authors would like to express their gratitude for projects supported by the National Natural Science Foundation of China (No. 52371077), Natural Science Foundation of Hebei Province (No. E2022203026), European Union's Research and Innovation Program Horizon Europe under the Marie Skłodowska-Curie Actions grant agreement (No. 101129996, SynAM) and UKRI Engineering and Physical Sciences Research Council.

Data availability

No data was used for the research described in the article.

References

[1]Q.H. Wang, S. Chang, H.W. Ding, et al., Electrochemical polishing process of additively manufactured IN738LC fine channels, Vacuum 240 (2025) 114564.

[2]C. Shen, Z.X. Pan, Y. Ma, et al., Fabrication of iron-rich Fe–Al intermetallics using the wire-arc additive manufacturing process, Addit. Manuf. 7 (2015) 20–26.

[3] H.Q. Zhang, K. Peng, W.J. Wu, et al., Efficient additive manufacturing of 2209 duplex stainless steel using multi-stranded wire plasma arc: numerical simulation, microstructure and mechanical properties, Vacuum 238 (2025) 114251.

[4] P. Kürnsteiner, P.B. Vila, P. Bajaj, et al., Designing an Fe-Ni-Ti maraging steel tailor-made for laser additive manufacturing, Addit. Manuf. 73 (2023) 103647.

[5] S. Liu, Z.J. Shi, X.L. Xing, et al., Effect of Nb additive on wear resistance and tensile properties of the hypereutectic Fe-Cr-C hard facing alloy, Mater. Today Commun. 24 (2020) 101232.

[6] W. Shao, Y.F. Zhou, L. Zhou, et al., Effect of Ti-doping on peeling resistance of primary M7C3 carbides in hypereutectic Fes-Cr-C hard facing coating and γ-Fe/ M7C3 interfacial bonding strength, Mater. Des. 211 (2021) 110133.

[7] T.H. Ding, C.N. Li, W. Jing, et al., Influences of boron on the microstructural characteristics and wear performance of hypereutectic Fe-Cr-C-Mo-xB hard facing alloy, Surf. Coating. Technol. 478 (2024) 130415.

[8] S. Liu, Y.F. Zhou, X.L. Xing, et al., Refining effect of TiC on primary M7C3 in hypereutectic Single bondCrsingle bondC harden-surface welding coating: experimental research and first-principles calculation, J. Alloys Compd. 691 (2017) 239–249.

[9]J.B. Wang, X.L. Xing, Y.F. Zhou, et al., Formation mechanism of ultrafine M7C3 carbide in a hypereutectic Fe-25Cr-4C-0.5Ti-0.5Nb-0.2N-2LaAlO3 hard facing alloy layer, J. Mater. Res. Technol. 9 (2020) 7711–7720.

[10]X. Yun, Y.F. Zhou, J. Yang, et al., Refinement of nano-Y2O3 on microstructure of hypereutectic Fe-Cr-C hard facing coatings, J. Rare Earths 33 (2015) 671–678.

[11]S. Liu, J. Zhang, Z.J. Wang, et al., Refinement and homogenization of M7C3 carbide in hypereutectic Fe-Cr-C coating by Y2O3 and TiC, Mater. Charact. 132 (2017)41–45.

[12]Y.H. Heng, Y.W. Mao, K.H. Feng, et al., Fine-grained binder jetted tungsten heavy alloys with in situ nano-La2O3 addition via a novel metal salt binder, Addit. Manuf. 109 (2025) 104843.

[13]Z.Y. Li, W.G. Chen, D.Y. Li, et al., Frictional wear properties of different nano La2O3 composite FeCoNiCrMo high-entropy alloy coatings under soil conditions, J. Mater. Res. Technol. 35 (2025) 6874–6888.

[14]Y.H. Chen, C.L. Yang, C.L. Fan, et al., Grain refinement of additive manufactured Ti-6.5Al-3.5Mo-1.5Zr-0.3Si titanium alloy by the addition of La2O3, Mater. Lett. 275 (2020) 128170.

[15]J. Yang, J.J. Tian, F.F. Hao, et al., Microstructure and wear resistance of the hypereutectic Fe-Cr-C alloy hard facing metals with different La2O3 additives, Appl. Surf. Sci. 289 (2014) 437–444.

[16]Y.N. He, J.B. Wang, T.F. Zhu, et al., Insights into refinement mechanism of primary M7C3 carbide by La2O3 via experiments and first-principles calculations, J. Mater. Res. Technol. 29 (2024) 4505–4513.

[17]Q. Wang, F.R. Liu, Atomic-scale bonding strength and failure mechanisms of HfC/ Ni/Ni3Al interfaces on low-index crystal planes: a combined HRTEM and first- principles study, Vacuum 230 (2024) 113658.

[18]J.T. Huang, Y. Liu, Z.H. Lai, et al., A systematic study of interface properties and fracture behaviour of graphene/aluminium: insights from a first-principles study, Vacuum 204 (2024) 111346.

[19]B.F. Chen, H. Wang, X.L. Li, et al., Atomic-scale design of Fe3C/α′C interfaces in carburized steels: first-principles insights into alloying doping for interfacial cohesion, Mater. Des. 254 (2025) 114099.

[20]W.Y. Huang, P. Wu, N. Chen, The behaviours of H atoms and vacancies at W/Lu2O3 interface: first-principles calculations, Appl. Surf. Sci. 693 (2025) 162777.

[21]H.Y. Hwang, Y. Iwasa, M. Kawasaki, et al., Emergent phenomena at oxide interfaces, Nat. Mater. 11 (2012) 103–113.

[22]L. Wang, Q. Wang, J. Huang, et al., Interface and interaction of graphene layers on SiC(000) covered with TiC(111) intercalation, Phys. Chem. Chem. Phys. 19 (2017) 26765–26772.

[23]G. Kresse, J. Hafner, Ab initio molecular dynamics for liquid metals, Phys. Rev. B 47 (1993) 558–561.

[24]J.P. Perdew, K. Burke, M. Ernzerhof, Generalized gradient approximation made simple, Phys. Rev. Lett. 77 (1996) 3865.

[25]D. Joubert, From ultrasoft pseudopotentials to the projector augmented-wave method, Phys. Rev. B Condens. Matter 59 (1999) 1758–1775.

[26]J.M. Wills, O. Eriksson, M. Alouani, in: Hugues Dreysse (Ed.), Electronic Structure and Physical Properties of Solids, Springer-Verlag, Berlin, 2000, p. 148.

[27]H. Skriver, The LMTO Method, Solid State Sciences, Springer-Verlag, Berlin, 1984, p. 85.

[28]H.W. Hugosson, P.A. Korzhavyi, U. Jansson, B. Johansson, Phase stabilities and structural relaxations in substoichiometric TiC1-x, Phys. Rev. B 63 (16) (2001) 165116.

[29]B.L. Bramfitt, The effect of carbide and nitride additions on the heterogeneous nucleation behaviour of liquid iron, Metall. Trans. A 1 (1970) 1987–1995.

[30]V. Fiorentini, M. Methfessel, Extracting convergent surface energies from slab calculations, J. Phys. Condens. Matter 8 (1996) 6525–6529.

[31]R. Li, B. Han, Z. Wang, et al., Effects of TiC addition on the interface stability, microstructure, and mechanical properties of IN718 fabricated by laser direct metal deposition: a combined experimental, DFT and MD study, Intermetallics 168 (2024) 108268.

[32]X. Guo, P. Yang, J. Zhang, et al., Effects of alloying element on the interface stability of fcc-Fe/NbC by first principles investigation, Vacuum 228 (2024) 113534.

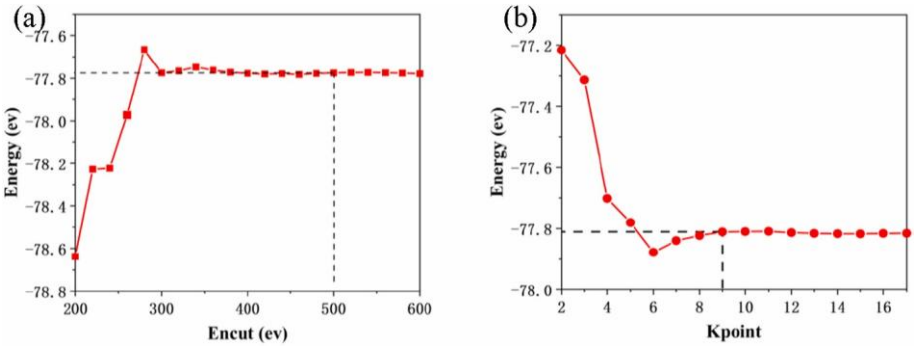

Fig. 1. Effect of Encut and K-point on the energy of the TiC: (a) Encut, (b) K-point.

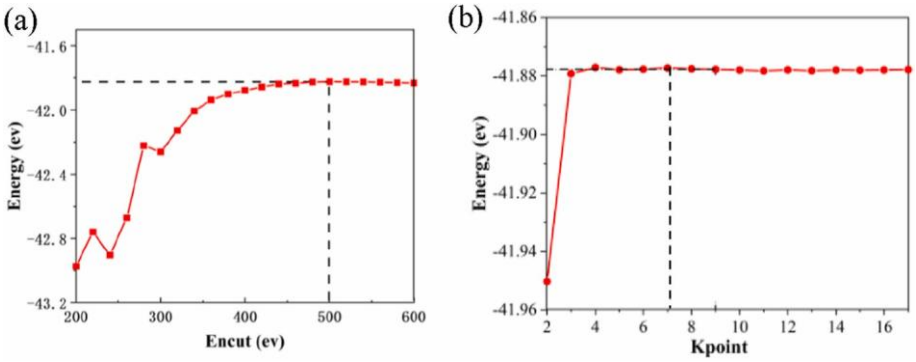

Fig. 2. Effect of Encut and K-point on the energy of the La_2O_3: (a) Encut, (b) K-point.

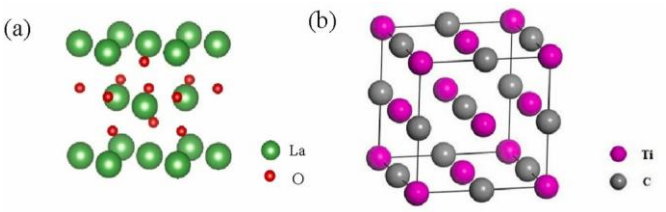

Fig. 3. Crystal structures of La_2O_3 and TiC: (a) La_2O_3, (b) TiC.

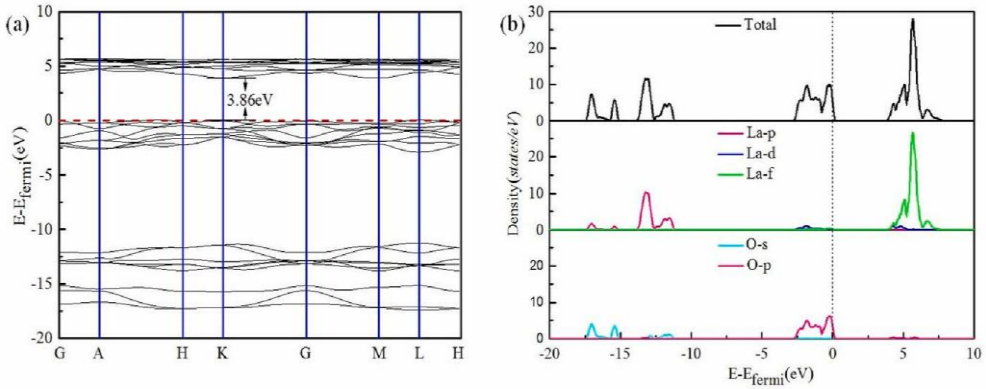

Fig. 4. Calculated phase properties of La_2O_3: (a) Energy band structure, (b) density of states diagram.

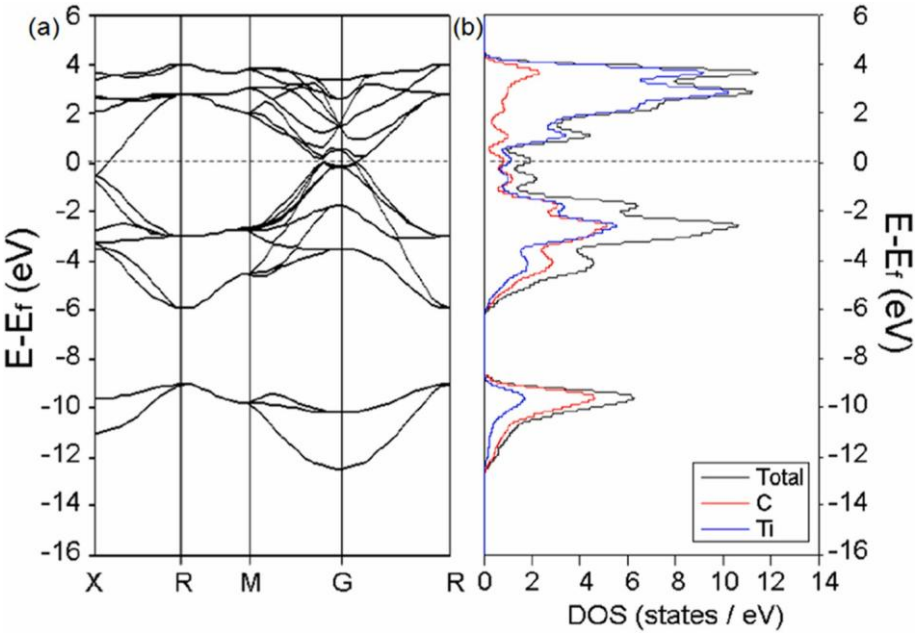

Fig. 5. Calculated phase properties of the TiC: (a) Energy band structure, (b) Density of states diagram.

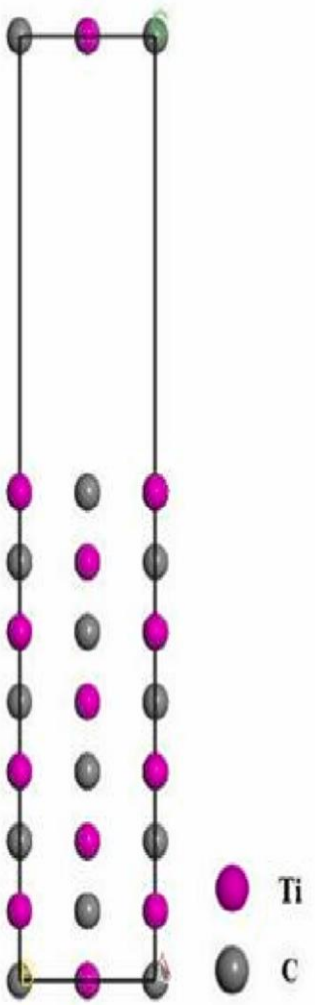

Fig. 6. TiC(1 ⊣ 0) surface model.

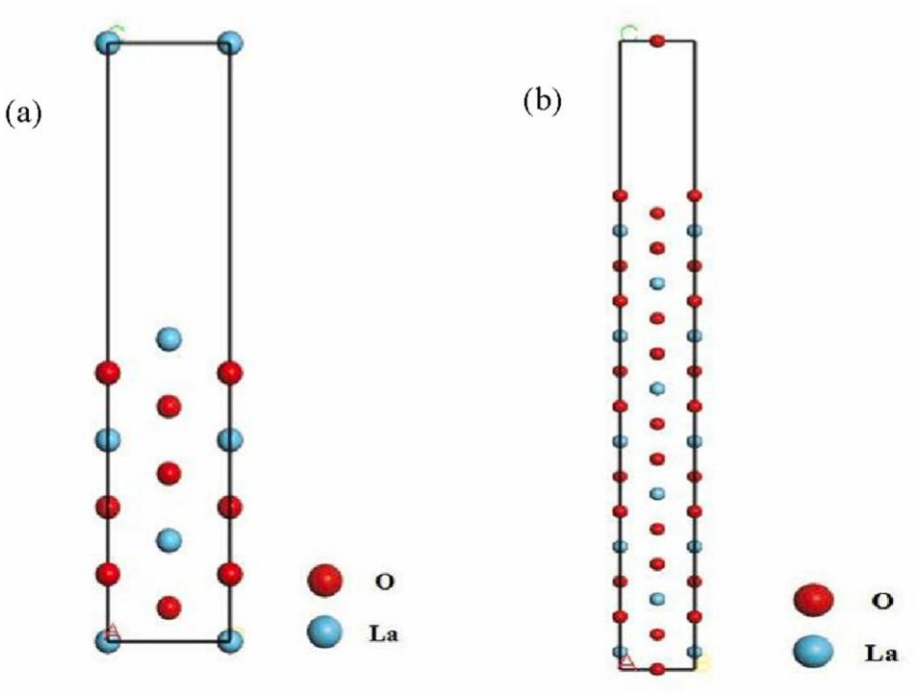

Fig. 7. $La_2O_3(1\bar{1}0)$ surface model with terminated surface atoms: (a) O-La atom termination, (b) O atom termination.

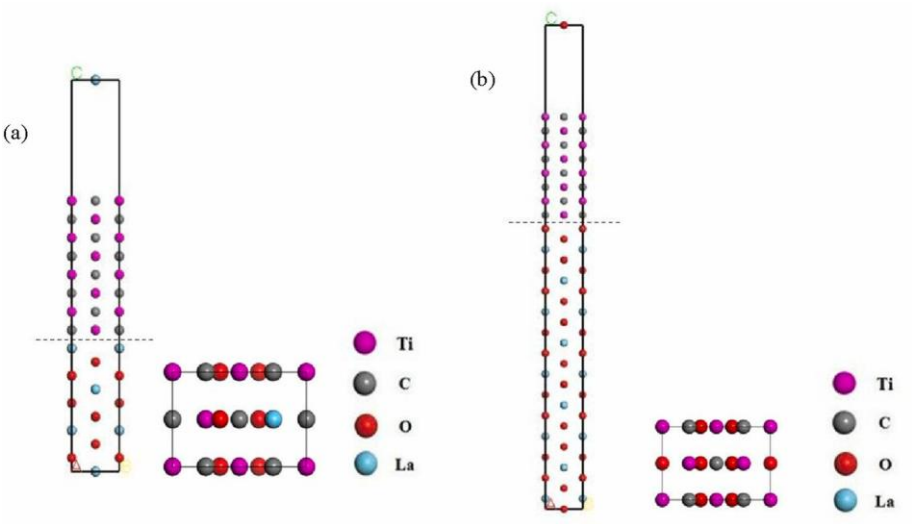

Fig. 8. Different termination-type interface models: (a) O-La atomic terminated model, (b) O atomic terminated model.

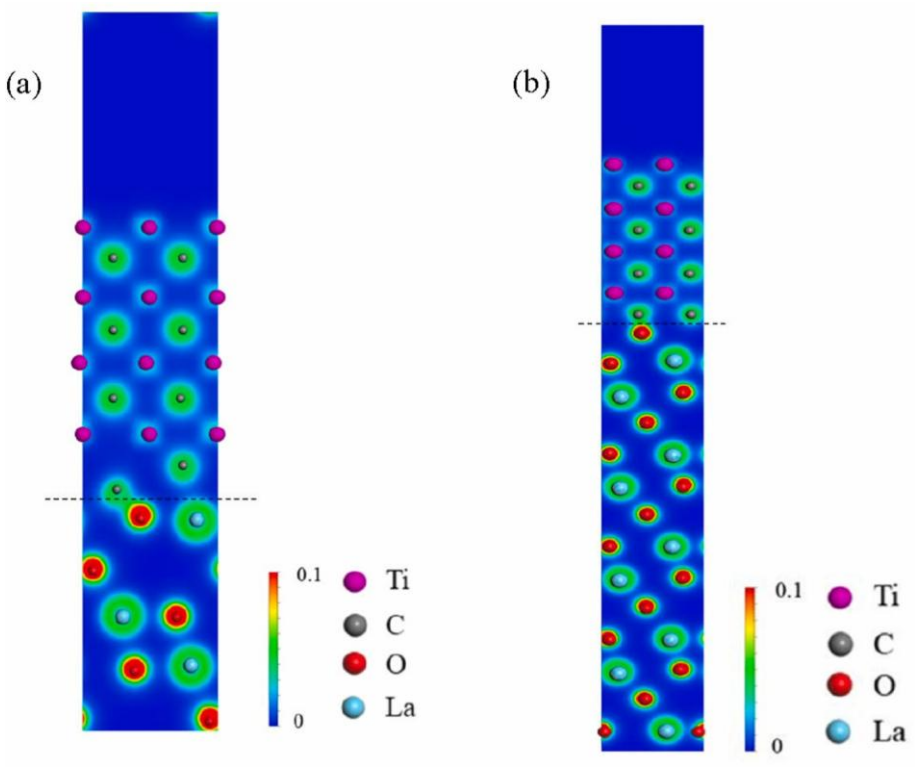

Fig. 9. Charge density of different termination-type interface models: (a) O-La atomic termination, (b) O atomic termination.

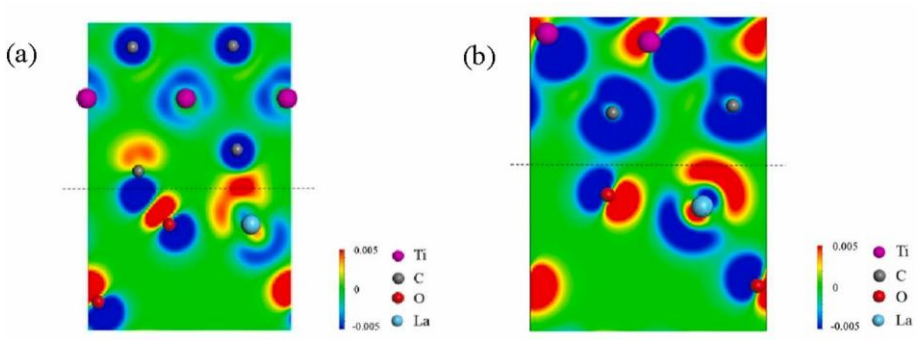

Fig. 10. Differential charge density of different termination-type interface models: (a) O-La atomic termination, (b) O atomic termination.

Table 1
Formation energies of TiC with different C vacancies.

Phase	No. of atoms	E_{form}(mRy/atom)
$TiC_{1.00}$	16	−65.8
$TiC_{0.90}$	15	−64.7
$TiC_{0.75}$	14	−58.8
$TiC_{0.63}$	13	−53.8

Table 2
Calculated results for mismatch degree of the low-index planes between La_2O_3 and TiC.

Selected crystal planes	$La_2O_3(1\ \bar{1}\ 0)$// $TiC(1\bar{1}\ 0)$	$La_2O_3(001)$//TiC (100)	$La_2O_3(110)$//TiC(1 $\bar{1}$ 0)
Mismatch degree (%)	4.10	22.28	26.06

Table 3
TiC(1 $\bar{1}$ 0) surface energy.

layers	6	7	8	9	10
Surface energy (J/m^2)	3.288	3.589	3.510	3.524	3.516

Table 4
$La_2O_3(1\ \bar{1}\ 0)$ surface energy of the O-La atomic-terminated surface model.

layers	4	7	10	13	16
Surface energy (J/m^2)	2.142	2.226	2.276	2.325	2.368

Table 5
$La_2O_3(1\ \bar{1}\ 0)$ surface energy of the O atomic-terminated surface model.

layers	19	22	25	28	31
Surface energy (J/m^2)	1.681	1.391	1.435	1.481	1.526

Table 6
W_{ad} of La_2O_3 $(1\bar{1}0)$/TiC $(1\bar{1}0)$ interface model with different termination conditions.

Termination in interface	$E_{La2_{O3}}$ (eV)	E_{TiC} (eV)	$E_{TiC/La2_{O3}}$ (eV)	w_{ad} ($J{\cdot}m^{-2}$)
O- termination	−379.07	−284.67	−658.99	$-1.88\ J\ m^{-2}$
O-La termination	−138.08	−284.67	−423.26	$0.51\ J\ m^{-2}$

Table 7

γ of La_2O_3 $(1\bar{1}0)$/TiC $(1\bar{1}0)$ interface model with different termination conditions.

Termination in interface	$\sigma_{La2_{O3}}$ (J·m^{-2})	σ_{TiC} (J·m^{-2})	γ (J·m^{-2})
O- termination	1.48 J m^{-2}	3.51 J m^{-2}	6.87 J m^{-2}
O-La termination	2.28 J m^{-2}	3.51 J m^{-2}	5.28 J m^{-2}